Journal of Information Hiding and Multimedia Signal Processing ©2023 ISSN 2073-4212
Ubiquitous International Volume **14**, Number **4**, December **2023**

Comparative Analysis and Practical Implementation of Sparse Arrays vs. Uniform Linear Arrays for Angle of Arrival Estimation Precision

Osama Ahmed Elkasrawi[1], Amr Mohamed Abdelaziz[2], Hossam El-Din Abou Bakr[3], Mohamed Atta Aboelazm[4]

[1 , 3 , 4] Department of Electronic Warfare, Military Technical College, Kobry ELkobba, Cairo, Egypt.
[2]Department of Communication, Military Technical College, Kobry ELkobba, Cairo, Egypt.

[1]osama.elkasrawi@gmail.com, [2]amrashry@mtc.edu.eg, [3]hossameldin_aboubakr@mtc.edu.eg, [4] mohamed.a.aboelazm@mtc.edu.eg

Correspond Author : mohamed.a.aboelazm@mtc.edu.eg
Received September 2023; revised November 2023, accepted December 2023

Abstract. Direction-Finding (DF) is a critical task in array signal processing for various applications such as radar, sonar, and wireless communication systems. Traditional Uniform Linear Arrays (ULAs) have been widely employed due to their simplicity and ease of implementation. However, ULAs suffer from limitations in terms of angular resolution, accuracy, mutual coupling, low signal-to-noise-ratio (SNR) scenarios, and dense environment handling. Sparse arrays, with their different types of configurations each having its pros and cons, have emerged as a promising alternative. In comparison to ULAs with an equal number of antenna elements, sparse arrays possess superior estimation performance in terms of accuracy and resolution. Consequently, this attribute leads to cost and complexity reduction, making sparse arrays highly valuable for various applications. This paper provides a comprehensive review of the fundamental principles of using sparse arrays for Angle of Arrival (AOA) estimation and compares the performance of the most common types. It then focuses on comparing the estimation performance of sparse arrays with ULAs based on of CramrRao bound (CRB) analysis. Theoretical analysis and simulation results demonstrate that sparse arrays outperform ULAs in terms of accuracy and angular resolution, providing strong support for their use in DF and highlighting its importance in real-world scenarios. To validate these findings, a prototype implementation using the National Instrument Universal Software Radio Peripheral (NI-USRP) Software Defined Radio (SDR) platform is developed to implement both sparse array-based and ULA-based DF and compare their performance. The experimental results yield in giving the best rating for sparse arrays over ULAs.
Keywords: AOA;Sparse; USRP; SDR ; MUSIC;Difference co-array.

1. **Introduction.** Accurate AOA estimation is crucial for many applications, such as radar, sonar, and wireless communication systems [1, 2]. Over the years, ULAs, consisting of equidistantly spaced antennas along a straight line, have been used for AOA estimation due to their simplicity and ease of implementation [1,3]. However, ULAs suffer from certain limitations that hinder their performance in certain scenarios. Insufficient angular resolution and diminished accuracy represent significant limitations associated with ULAs, particularly when dealing with closely spaced sources or a reduced number of array elements. Therefore, to attain great accuracy, numerous antenna elements are

needed, which can be expensive and computationally complex [4, 5]. In practical applications, the use of ULAs for AOA estimation is also impacted by mutual coupling between the antenna elements [6]. This coupling can significantly affect the accuracy of AOA estimation [6, 7]. Several methods, relying on an assumed mutual-coupling model, attempt to eliminate the mutual coupling impact from acquired data. However, these methods are computationally intensive and can be susceptible to errors caused by disparities between the actual system and the used model [8]. Another limitation for ULAs is the inability to deal with dense environments in which the number of sources exceeds the number of elements in the array [3–5]. Due to these limitations, sparse array-based DF has emerged as a promising alternative that gained great attention in recent years [9–11]. Sparse arrays offer significant benefits over ULA in effectively addressing mutual coupling effects. Through a thoughtfully designed arrangement of antenna elements in sparse arrays, the inter-element spacing is increased, resulting in reduced mutual coupling between neighboring antennas. Consequently, sparse arrays are well-suited for applications where minimizing mutual coupling is essential, leading to enhanced array sensitivity and improved array performance in practical scenarios [9, 10]. Moreover, due to their larger aperture and the higher degree of freedom sparse arrays can maintain higher resolution and accuracy with a reduced number of antennas, particularly in low SNR situations, resulting in a lower cost, and complexity [9–11]. Sparse arrays come in several types, including Minimum-Redundancy-Array (MRA), Coprime-Array (COA), Nested-Array (NA), and Super-Nested-Array (SNA) [9,10,12,13]. MRA achieves a greater aperture and higher degree-of-freedom (DOF) by maximizing the number of consecutive lags in the difference co-array (DCA) while minimizing redundancies [10, 14]. However, due to the absence of a closed-form expression for the MRA configuration, designing the array is challenging [13–15]. COA has a sparse structure with a relatively large aperture and lower mutual coupling effect, but the DCA contains holes that reduce the effective degree of freedom [12, 14, 15]. NA is designed to increase the aperture and achieve a higher degree of freedom in AOA estimation, but it has a greater mutual coupling effect due to a large number of antenna elements with a unit inter-element spacing [10]. SNA combines the advantages of all of these types. It has the same DCA properties as NA but with a more sparse structure, resulting in a lower mutual coupling effect [10, 14, 15]. This paper explores the viability of employing sparse arrays as an alternative to using ULAs in AOA estimation. The investigation includes comprehensive simulation analysis and practical verification, demonstrating the superior estimation performance of sparse arrays when compared to ULAs. At first, this study reviews the fundamental principles of using sparse arrays for AOA estimation and explore the performance of different types of sparse arrays. Then the performance of these arrays is compared to the ULAs. Theoretical and simulation analysis indicates that MRA and SNA offer superior performance compared to NA and COA. Furthermore, the simulation results reveal that sparse arrays provide better resolution, accuracy and lower mutual coupling than ULAs. Finally, in order to support the simulation results, we have built a prototype implementation using SDR technology. The experimental results demonstrate that the $3dB$ beam-width (BW) is smaller for sparse arrays than for a ULA, indicating improved resolution and accuracy. The rest of this paper is organized as follows: Section 2 discusses the fundamentals and the signal modeling for sparse array-based AOA estimation, explores the different types of sparse arrays and compares them theoretically. Furthermore, It incorporates a comparison between ULAs and sparse arrays in terms of CRB, serving as a crucial metric parameter for assessing and contrasting estimation performance. Section 3 presents a simulation-based analysis that corroborates the findings derived from the theoretical investigation. The simulation analysis specifically focuses on comparing the AOA estimation performance

using both ULAs and sparse arrays. Theoretical and simulation analysis can help in choosing the optimal sparse array type to implement, taking into account the available laboratory hardware limitations, for comparison with ULA. Section 4 introduces the practical verification of the results obtained from the theoretical and simulation investigations. It provides comprehensive details on the practical implementation of both ULAs and the selected sparse array type using the NI-USRP SDR platform for the purpose of assessing and contrasting their respective performances. Finally, the paper is concluded in Section 5.

2. Sparse array-based direction finding.

2.1. Signal model.

Assume M narrow band far-field Signal-of-Interest (SOI) impinging on an antenna array with N physical elements where elements locations are equal to n times of d with n belonging to integer set $\mathbb{P}$ that represents the normalized sensors locations and $d = \frac{\lambda}{2}$ denotes the inter-element spacing. The propagation channel is assumed to be a White-Gaussian-Noise channel (AWGN) in which noise samples are i.i.d and has normalized Gaussian distribution $\sim \mathcal{N}(0, \sigma^2)$. The received signal $\mathbf{x}_{\mathbb{P}}$ can be modeled as follows:

$$\mathbf{x}_{\mathbb{P}} = \sum_{i=1}^{M} A\mathbf{s}_{\mathbb{P}}(\theta_i) + \mathbf{n} \tag{1}$$

Where $\mathbf{n}$ is the noise term, θ_i represents i^{th} source AOA ,A_i is the i^{th} signal amplitude and $\mathbf{s}_{\mathbb{P}}(\theta_i) = \left[e^{j\frac{2\pi}{\lambda}nd\sin\theta_i}\right]_{n\in\mathbb{P}}$ is the steering vector associated with θ_i. We also assume that SOIs and noise are uncorrelated. From (1),covariance matrix can be represented as follows:

$$\mathbf{R} = \sum_{i=1}^{M} A_i^2\mathbf{s}_{\mathbb{P}}(\theta_i)\mathbf{s}_{\mathbb{P}}^H(\theta_i) + \sigma^2\mathbf{I} \tag{2}$$

The product term $\mathbf{s}_{\mathbb{P}}(\theta_i)\mathbf{s}_{\mathbb{P}}^H(\theta_i)$ in (2) can be modeled as $e^{j\frac{2\pi}{\lambda}(n_1-n_2)d\sin\theta_i}$ where n_1,$n_2 \in \mathbb{P}$. This indicates that while determining the correlation matrix, the distance between the sensor locations has a more critical effect than the actual sensor locations themselves [10, 12]. As a result, the correlation matrix can be converted into a correlation vector by using the Kronecker product [9, 10, 12], as expressed below:

$$\begin{aligned}\mathbf{x}_{\mathbb{V}} &= \mathrm{vec}(\mathbf{R}) \\ &= \sum_{i=1}^{M} A_i^2\mathbf{s}_{\mathbb{V}}(\theta_i) + \sigma^2\tilde{\mathbf{I}}\end{aligned} \tag{3}$$

Where $\tilde{\mathbf{I}} = \mathrm{vec}(\mathbf{I})$ and $\mathbf{s}_{\mathbb{V}}(\theta_i) = \left[e^{j\frac{2\pi}{\lambda}(n_1-n_2)d\sin\theta_i}\right]_{n_1,n_2\in\mathbb{P}}$ $n_1 - n_2 = m \in \mathbb{V}$ with $\mathbb{V}$ defined as the DCA of the array $\mathbb{P}$, which can be expressed as follows: Let the normalized sensors locations in a sparse array are defined by the integer set $\mathbb{P}$, then the DCA can be formulated as follows:

$$\mathbb{V} = \{n_j - n_q | j, q \in \mathbb{P}\} \tag{4}$$

Simply the distinct entries of $\mathbb{V}$ is obtained by subtracting all possible sensor locations in the given sparse array and DCA is then formed by considering only the non-repeating differences [13, 14]. Based on the definition of the DCA, some new definitions can be deduced as follows : [13, 14]

- Central uniform linear array segment (CULA): It is regarded as the largest continuous central section of the DCA that doesn't have any holes in it. Throughout this paper, CULA is denoted by the symbol $\mathbb{U}$.

- Uniform Degree of Freedom (UDOF): A more useful parameter, which is denoted by the symbol ξ, indicates the number of continuous entries in the DCA .
- Restricted array: If the DCA of an array is hole-free, the array is said to be a restricted array.

By comparing (1) with (3), $\mathbf{x}_{\mathbb{V}}$ in (3) can be assumed to represent the signal received from an antenna array with a new array-manifold $\mathbf{S}_{\mathbb{V}}$=$[\mathbf{s}_{\mathbb{V}}(\theta_1), ..., \mathbf{s}_{\mathbb{V}}(\theta_M)]$ which represents a manifold of a larger array with sensors locations determined by the DCA. The DCA output, $\mathbf{x}_{\mathbb{V}}$, contains only one snapshot resulting in a rank-one covariance matrix. As a consequence, subspace-decomposition algorithms cannot be employed for AOA estimation [9, 12]. In this paper, the spatial smoothing strategy is used to generate a positive semi-definite matrix with a big enough rank that is a need for applying subspace-decomposition algorithms for AOA estimation [12]. Consequently, the virtual ULA is first split into L overlapping uniform sub-arrays each with a size of L elements [16] and the output output of the l^{th} sub-array is defined as follows [16]:

$$\mathbf{y}_l = \Upsilon_l \mathbf{x}_{\mathbb{V}} \tag{5}$$

Where $l = 1, 2, ..., L$ and Υ_l represents the selection matrix for the l^{th} sub-array which can be formulated as follows:

$$\Upsilon_l = \left[\mathbf{0}_{L\times(l-1)}\ \mathbf{I}_{L\times L}\ \mathbf{0}_{L\times(L-l)}\right] \tag{6}$$

Consequently, the definition of the covariance matrix that is resulted from using the spatial smoothing strategy can be defined as follows [9, 16]:

$$\mathbf{R}_{\mathbb{V}} = \frac{1}{L}\sum_{l=1}^{L} \mathbf{y}_l {\mathbf{y}_l}^H \tag{7}$$

Thus, the spatially smoothed covariance matrix $\mathbf{R}_{\mathbb{V}}$ can be used with the MUSIC algorithm, one of the subspace-decomposition algorithms, to perform AOA estimation as expressed by the following equation [9, 10]:

$$P_{MUS}(\theta) = \frac{1}{a^H(\theta) Q_n Q_n^H a(\theta)} \tag{8}$$

Where Q_n and $a^H(\theta)$ represent noise-subspace eigenvectors and the steering vector, respectively.

2.2. **Various sparse array types.** A sparse array will raise the DOF, which will be closer to $N(N-1)$, for any array structure [14]. As a result, the array should perform better than a ULA with the same length and detect a larger number of sources. Alternately, the same ULA performance could be obtained with fewer sensors in sparse array which lead to lower cost, weight, computational complexity ... etc. Along with increasing the DOF, sparse-arrays can aid in lowering the mutual coupling effect, which in turn improves estimation performance [10, 14]. Sparse arrays come in a several types, but here we'll focus on the most common and significant ones [9, 10, 13, 14]. Figure 1 illustrates physical elements' normalized locations and the DCA of the sparse array geometries under concern.

2.2.1. *Minimum-Redundancy-Array (MRA).* In a MRA, the goal is to maximize the DCA while minimizing the number of redundancies and preventing the introduction of any holes into the co-array [14, 17]. Since MRAs lack closed-form expressions, finding the ideal array and figuring out the ideal sensor locations necessitate an exhaustive search [9].

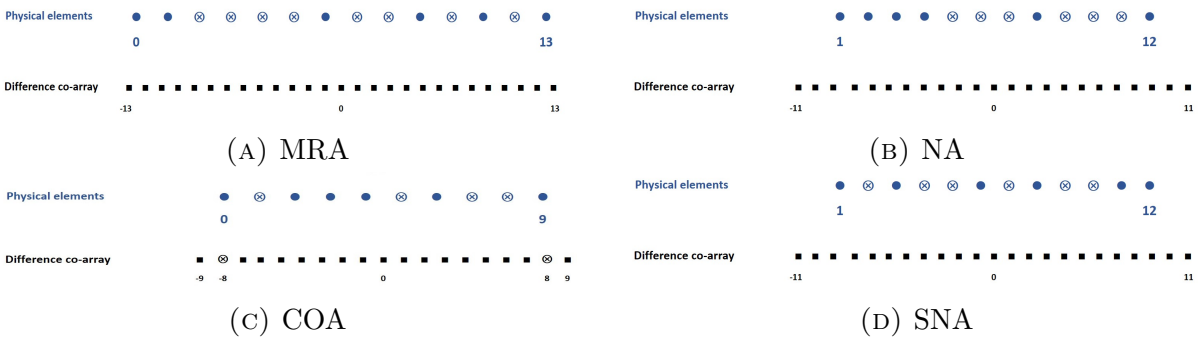

(A) MRA (B) NA

(C) COA (D) SNA

FIGURE 1. Different sparse array geometries. Blue dots denote physical sensors and blue crosses represent the empty positions in the physical layer. Black squares denote DCA elements and black crosses denote DCA holes. Number of physical sensors, for illustration, is assumed to equal 6 sensors

The following equation represents the optimization problem to determine sensor locations in MRAs [13, 17].

$$\begin{aligned} \underset{\mathbb{P}_{MRA}}{\text{maximize}} \quad & |\mathbb{V}| \\ \text{subject to} \quad & |\mathbb{P}_{MRA}| = N, \mathbb{V} = \mathbb{U} \end{aligned} \tag{9}$$

Where $\mathbb{P}_{MRA}$ denotes the MRA sensor locations. In terms of the maximum number of consecutive lags and hole-free co-arrays, MRA is optimal for a given number of sensors, but it is challenging to locate these sensors [13,14]. For scenarios, especially when a larger array of sensors needs to be created, extracting sensors locations requires a lookup table or advanced search, neither of which is practical [14].

2.2.2. *Nested-Array (NA).* It offers a higher DOF than ULAs, but less than MRAs, while having a closed-form equation for the array geometry [9,14].NA is consisted of two uniform linear sub-arrays, one of which is a dense array with N_1 sensors and inter-element spacing of $d = \frac{\lambda}{2}$, while the other is more sparsely spaced with N_2 sensors and inter-element spacing of $(N_1 + 1)d$ [13, 17]. NA follows the following equation for determining the normalized sensors' positions [17].

$$\mathbb{P}_{NA} = \{1, 2, ..., N_1, (N_1 + 1), 2(N_1 + 1), ..., N_2(N_1 + 1)\} \tag{10}$$

NA geometry has the benefit of having a simple design equation that is helpful for creating arrays with so many elements. Another benefit of NA is that there are no holes in its DCA, which is made up of continuous integers from $-N_2(N_1+1)+1$ to $N_2(N_1+1)-1$ [17]. The mutual coupling between neighboring antenna elements of NA becomes considerable and impairs the AOA estimation accuracy as the number of sensors which are separated by only unit inter-element spacing increases and this is thought to be the major drawback of the NA design [14].

2.2.3. *Coprime-Array (COA).* COA is made up of two ULAs with sensor separations of G and U, where G and U are coprime integers and $G < U$ [13,17]. It is simple in design and features the following closed-form equation for the normalized sensor position [12, 13, 17].

$$\mathbb{P}_{COA} = \{0, G, 2G, ..., (U - 1)G, U, 2U, ..., (2G - 1)U\} \tag{11}$$

The COA's DCA actually has a maximum CULA segment from $-(GU + G - 1)$ to $(GU + G - 1)$, with hole positions outside of this range [14, 17]. The COA's geometry drawback is that its DCA is not hole-free, which means it presents less DOF than the

nested array [12, 13, 17]. However, when the mutual coupling is a significant issue, COAs are preferred because they allow for a wider neighboring sensor spacing [12, 17].

2.2.4. *Super-Nested-Array (SNA).* Given the benefits and drawbacks of the sparse array types previously discussed, there was a need for an alternative array geometry that satisfies the following characteristics

- DCA should have a large CULA with no holes.
- The sensors' location must be described by a straightforward equation.
- The array should have a smaller number of sensor pairs with strong mutual coupling and inter-element spacing equal to d.

All of these features are achieved in the SNA [13, 14, 17]. SNA uses the following formula to determine the normalized sensors' locations [10, 14].

$$\mathbb{P}_{SNA} = \mathbb{S}_1 \cup \mathbb{Q}_1 \cup \mathbb{S}_2 \cup \mathbb{Q}_2 \cup \mathbb{T}_1 \cup \mathbb{T}_2 \tag{12}$$

where

$$\begin{gathered}
\mathbb{S}_1 = \{1 + 2r \ \ ; 0 \leq r \leq \chi_1\} \\
\mathbb{Q}_1 = \{(N_1 + 1) - (1 + 2r) \ \ ; 0 \leq r \leq \beta_1\} \\
\mathbb{S}_2 = \{(N_1 + 1) + (2 + 2r) \ \ ; 0 \leq r \leq \chi_2\} \\
\mathbb{Q}_2 = \{2(N_1 + 1) - (2 + 2r) \ \ ; 0 \leq r \leq \beta_2\} \\
\mathbb{T}_1 = \{r(N_1 + 1) \ \ ; 2 \leq r \leq N_2\} \\
\mathbb{T}_2 = \{N_2(N_1 + 1) - 1\}
\end{gathered}$$

with

$$\begin{gathered}
(\chi_1, \beta_1, \chi_2, \beta_2) = (f, f-1, f-1, f-2) \quad for\ N_1 = 4f \\
(\chi_1, \beta_1, \chi_2, \beta_2) = (f, f-1, f-1, f-1) \quad for\ N_1 = 4f+1 \\
(\chi_1, \beta_1, \chi_2, \beta_2) = (f+1, f-1, f, f-2) \quad for\ N_1 = 4f+2 \\
(\chi_1, \beta_1, \chi_2, \beta_2) = (f, f, f, f-1) \quad for\ N_1 = 4f+3
\end{gathered}$$

where f is an integer and $(N_1 + N_2)$ represents the total number of physical elements. The best option for N1 and N2 is to be evenly distributed [18]. From (12), SNA geometry is created by making the following changes to its parents' NA geometery. It is necessary to redesign the dense sub-array by omitting some sensors and carefully reallocating them to avoid the mutual coupling effect that emerged as a result of the NA's dense sub-array [10,13,14]. The dense sub-array elements are split into four sub-arrays, each with an element spacing of $2d$ and then the sensor at position $N_1 + 1$ is shifted to $N_2(N_1 + 1) - 1$. As a result, SNA dramatically reduces the number of sensor pairs with separation d. Consequently, SNA is thought to be more sparse than NA,and hence lowers the mutual coupling effect [10, 13, 14]. SNA has the same co-array as the NA but with modified normalized sensor location [10, 14]. As its DCA has no holes, SNA is widely known to be a restricted array [10, 14].

2.3. **CRB analysis.** The CRB plays a crucial role in the estimation process by providing the fundamental limit on the achievable accuracy of parameter estimation [19].The CRB enables researchers to assess the impact of various factors, such as noise levels, signal characteristics, and array configurations, on the accuracy and resolution of the estimation process [9, 19, 20]. In [19], CRB equation was proposed to account for scenarios where the

number of sources is either smaller or greater than the number of elements in the array. The equation can be expressed as follows:

$$CRB(\theta) = \frac{1}{4\pi^2 D}\left(\mathbf{B}_0^H \mathbf{\Pi}^{\perp}_{\mathbf{CK}_{\mathbb{V}}} \mathbf{B}_0\right)^{-1} \tag{13}$$

Where,

$$\mathbf{B}_0 = \mathbf{C}(diag(\mathbb{V})) \times \mathbf{S}_{\mathbb{V}} \times (diag(p_1, p_2, ..., p_M)) \tag{14}$$

$$\mathbf{C} = (\mathbf{J}^H(\mathbf{R}^T \otimes \mathbf{R})^{-1}\mathbf{J})^{\frac{1}{2}} \tag{15}$$

After simple mathematical manipulation to express several SOIs with different powers, $\mathbf{R}$ in equation (2) can be written as follows:

$$\mathbf{R} = \sum_{i=1}^{M} p_i \mathbf{s}_{\mathbb{P}}(\theta_i)\mathbf{s}^H_{\mathbb{P}}(\theta_i) + p_n \mathbf{I} \tag{16}$$

$$\mathbf{S}_{\mathbb{V}} = [\mathbf{s}_{\mathbb{V}}(\theta_1) \;\; \mathbf{s}_{\mathbb{V}}(\theta_2) \;\; .... \;\; \mathbf{s}_{\mathbb{V}}(\theta_M)] \tag{17}$$

$$\mathbf{K}_{\mathbb{V}} = [\mathbf{S}_{\mathbb{V}} \;\; \mathbf{e}_0] \tag{18}$$

where D,M,p_n and p_i are the total number of snapshots, number of sources, noise power and the i^{th} source power, with $i = 1, 2, \; .... \; , M$, respectively. The matrix $\mathbf{J}$, which had been explained in detail in appendix "B" in [19], is a binary matrix with size $|\mathbb{P}|^2$ by $|\mathbb{V}|$ with its column that is associated with the difference m is given by:

$$\langle \mathbf{J} \rangle_{:,m} = \text{vec}(\mathbf{I}(m)) \qquad\qquad , m \in \mathbb{V} \tag{19}$$

where the matrix $\mathbf{I}(m)$ has a size of $|\mathbb{P}|$ by $|\mathbb{P}|$ and satisfies the following condition:

$$\langle \mathbf{I}(m) \rangle_{n_1,n_2} = \begin{cases} 1, & if \; n_1 - n_2 = m, \\ 0, & otherwise. \end{cases} \;\; , \; n_1, n_2 \in \mathbb{P} \tag{20}$$

Substituting $\mathbf{CK}_{\mathbb{V}} = \mathbf{\Delta}$, the matrix $\mathbf{\Pi}^{\perp}_{\mathbf{CK}_{\mathbb{V}}}$ becomes equivalent to the matrix $\mathbf{\Pi}^{\perp}_{\mathbf{\Delta}}$. The matrix $\mathbf{\Pi}^{\perp}_{\mathbf{\Delta}}$ can be computed through the following equation, discussed in detail in [19]

$$\mathbf{\Pi}^{\perp}_{\mathbf{\Delta}} = \mathbf{I} - \mathbf{\Delta}(\mathbf{\Delta^H \Delta})^{-1}\mathbf{\Delta^H} \tag{21}$$

The symbol $\mathbf{e}_0$ represents a column vector such that $\mathbf{e}_0 \in \{0, 1\}^{|\mathbb{V}|}$ satisfying the following condition:

$$\langle \mathbf{e}_0 \rangle_m = \begin{cases} 1, & if \; m = 0, \\ 0, & otherwise. \end{cases} \;\; , \; m \in \mathbb{V} \tag{22}$$

The term $\mathbf{B}_0$ is dependent on the characteristics of the DCA and its length, while the term $\mathbf{C}$ is influenced by the array configuration $\mathbb{P}$, which encompasses the physical elements' positions. Therefore, the array configuration, characteristics, and length of the DCA have a significant inverse impact on the CRB [9, 19]. Sparse arrays characterized by a sparser array configuration $\mathbb{P}$, result in a larger array aperture, and a larger DCA [9, 11, 13, 14]. Consequently, based on (13) to (18), sparse arrays exhibit a reduced CRB compared to ULAs when considering an equal number of sources. This indicates that sparse arrays provide superior resolution and accuracy in AOA estimation compared to ULAs [9,20,21].

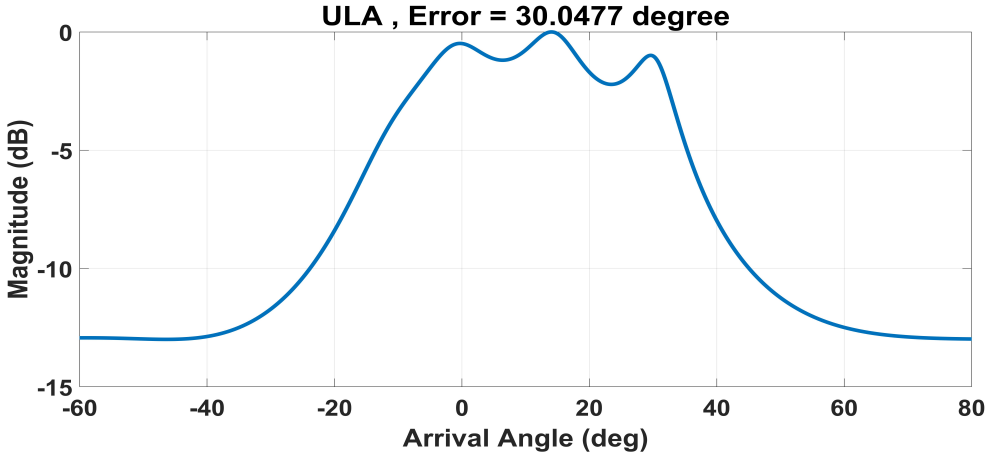

FIGURE 2. MUSIC pseudo-spectrum using ULA.

3. **Simulation Analysis.** MATLAB-based simulation analysis is conducted to evaluate the performance of sparse arrays in AOA estimation and compare their estimation performance capabilities with traditional ULAs. We assume four narrow-band non-coherent sources with their respective AOAs being $[0°, 10°, 20°, 30°]$. We consider signal propagation over an AWGN channel with an assumed SNR of 0 dB. The number of snapshots equals 1000 snapshot. The array comprises a total of 6 physical elements, which are distributed according to each array type. For instance, As illustrated in figure 1a the sensor locations for MRA are given by $\mathbb{P}_{MRA}$= $\{0, 1, 6, 9, , 11, 13\}$ as mentioned in [10]. Consequently, its DCA, $\mathbb{V}$, extends from -13 to 13, without any holes. Notably, this leads to CULA, $\mathbb{U}$, ranging from -13 to 13 resulting in a UDOF ξ=27. Accordingly, the maximum number of sources that can be identified is $(\xi - 1)/2$ =13 source [14, 17]. Similarly, for NA with N_1=N_2=3 the sensor locations, which are derived using (10), are given by $\mathbb{P}_{NA}$= $\{1, 2, 3, 4, 8, 12\}$ as shown in figure 1b. This leads to $\mathbb{V}$ that extends from -11 to 11 with no holes. Consequently, $\mathbb{U}$ ranges from -11 to 11 resulting in ξ=23 which enables detection of 11 sources at maximum. In case of COA with G=2 and U=3 the sensor locations are obtained from (11), giving $\mathbb{P}_{COA}$= $\{0, 2, 4, 3, 6, 9\}$ as illustrated in figure 1c. As a result, $\mathbb{V}$ extends from -9 to 9 with holes at position -8 and 8. This leads to $\mathbb{U}$ that ranges from -7 to 7, resulting in ξ=15 and enabling the detection of a maximum of 7 sources. Figure 1d, displays SNA with sensor locations $\mathbb{P}_{SNA}$= $\{1, 3, 6, 8, 11, 12\}$ according to (12). $\mathbb{V}$ extends from -11 to 11 with no holes leading to $\mathbb{U}$ ranges from -11 to 11. Consequently, it has ξ=23, enabling the detection of a maximum of 11 sources at maximum.

Finally, the ULA sensor locations is given by $\mathbb{P}_{ULA}$= $\{0, 1, 2, 3, 4, 5\}$, resulting in $\mathbb{V}$ that extends from -5 to 5 with no holes making $\mathbb{U}$ has the same range and hence $\xi = 11$ which allow detection of 5 sources at maximum. The estimation accuracy and resolution for the previously mentioned sparse arrays are assessed in this simulation. Mutual coupling contaminates SOIs and the DF process is carried out immediately without the use of any decoupling techniques. RMSE of the estimated AOA can be described as follows [17]

$$RMSE = \sqrt{\frac{1}{M}\sum_{t=1}^{M}(\widetilde{\theta}_t - \theta_t)^2} \tag{23}$$

Where $\widetilde{\theta}_t$ represents the estimation of the real angle θ_t, while M denotes the total number of sources impinged on the array. Figure 2 demonstrates how inaccurately ULA identifies

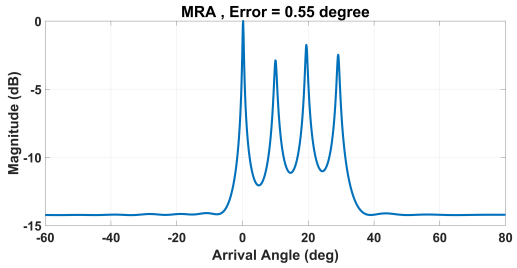

FIGURE 3. MUSIC pseudo-spectrum using MRA.

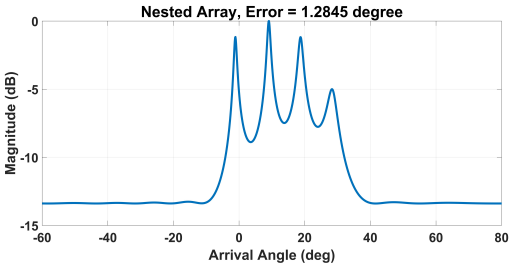

FIGURE 4. MUSIC pseudo-spectrum using NA.

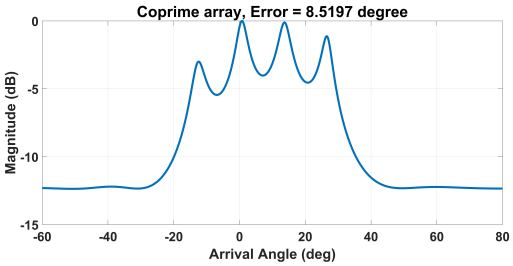

FIGURE 5. MUSIC pseudo-spectrum using COA.

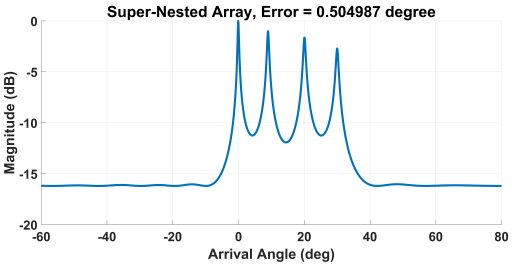

FIGURE 6. MUSIC pseudo-spectrum using SNA.

the four peaks related to the SOIs. It achieves 30.0477° RMSE. Figure 3 and 6 show that in terms of resolution and accuracy, MRA and SNA have the best estimation performance. For MRA and SNA, the RMSE values were 0.55° and 0.504°, respectively. Both NA and COA can detect SOIs peaks as shown in figure 4 and 5, but with greater estimating error, achieving RMSE values of 1.28° and 8.52°, respectively. These results show that SNA has the best-estimating performance in terms of accuracy and resolution followed by MRA, NA, and COA in that order and finally, ULAs demonstrate the least favorable performance. This gives preference to using sparse arrays over ULAs.

4. **Experimental Results.** Theoretical analysis and simulation results both support the assertion that AOA estimation using SNA has the best estimation performance, followed by MRA. Based on these findings and the limited resources in our laboratory, MRA was chosen to be implemented. In this section, we develop a prototype based on the NI-USRP SDR platform for AOA estimate utilizing MRA, as shown in figure 7a and 8a , and evaluate its performance in comparison to the outcomes of ULA-based estimation as illustrated in figure 7b and 8b. Figure 7 represents the schematic block diagram of DF experiential setup, in which one USRP-2930 is employed as an SOI transmitter and four USRPs-2930 form a four-channel RF receiver. Phase synchronization and the calibration procedure are carried out using an additional USRP-2930 and an external clock distributor (Octoclock) to eliminate the constant relative phase offsets that exist between receive channels. In our prior publication [22], we described phase synchronization and the calibration procedure steps in detail. Table 1 contains a list of the used components in DF experiment setup.

In contrast to MRA, which has a non-uniform spacing between the elements as shown in figure 7a, ULA has a uniform spacing between every two succeeding elements $d = \frac{\lambda}{2}$ as illustrated in figure 7b. As shown in figure 8,Both the MRA-based and ULA-based DF functional block diagram, which illustrates the data flow and processes of LabVIEW-based DF receiver design code, in figure 8, have four loops in order to speed up the processing.

- **The parameters identification loop:** takes reception parameters and filter coefficients as inputs. It also includes the array geometry designing steps.

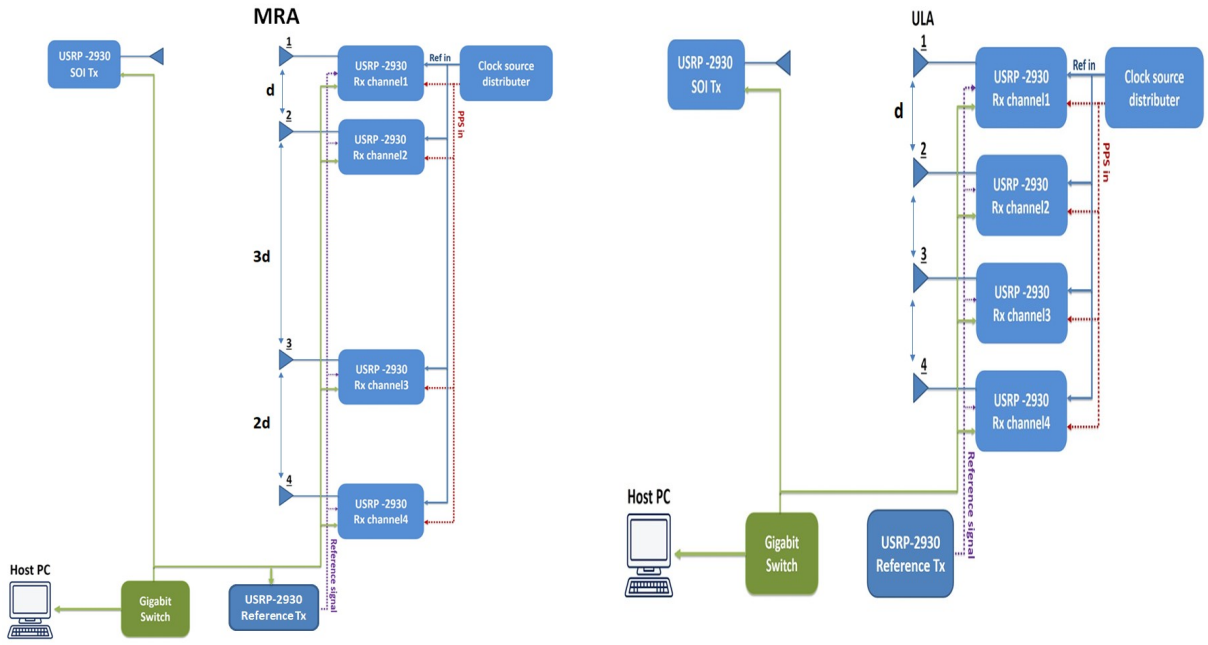

(A) Sparse array (B) ULA

FIGURE 7. Experiment schematic block-diagram

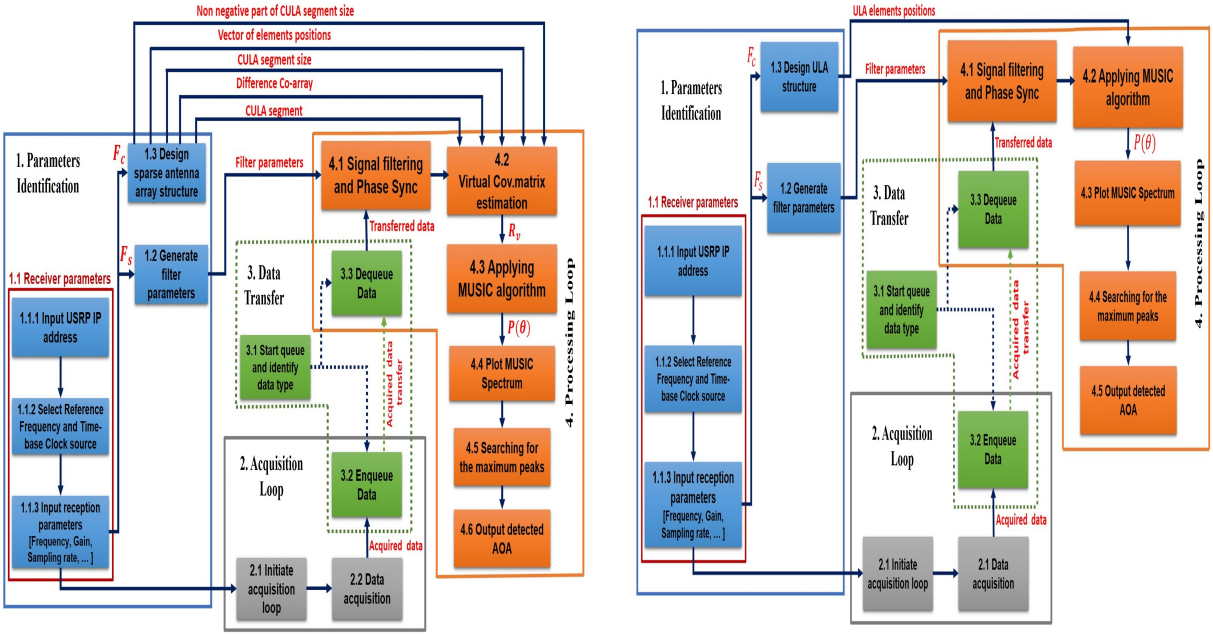

(A) DF using Sparse array (B) DF using ULA

FIGURE 8. LabVIEW-based DF receiver functional block diagram

- **The acquisition loop:** starts the USRP session so that the signal acquisition can be performed.
- **Processing loop:** phase synchronization, SOI filtering and AOA estimation steps are all applied in this loop.
- **Data transfer loop:** in which received data is transferred from the acquisition loop to the processing loop.

Figure 8b represents the functional block diagram, which illustrates the data flow and processes of LabVIEW-based DF receiver design code, utilized with the USRP-2930 platform after a variety of adjustments for ULA-based DF, as we demonstrate in our earlier paper [22]. The newly constructed DF receiver functional block diagram for sparse array-based DF is shown in Figure 8a, where the processing loop and the parameters identification loop are adjusted as follows. At first, we add a "design sparse antenna

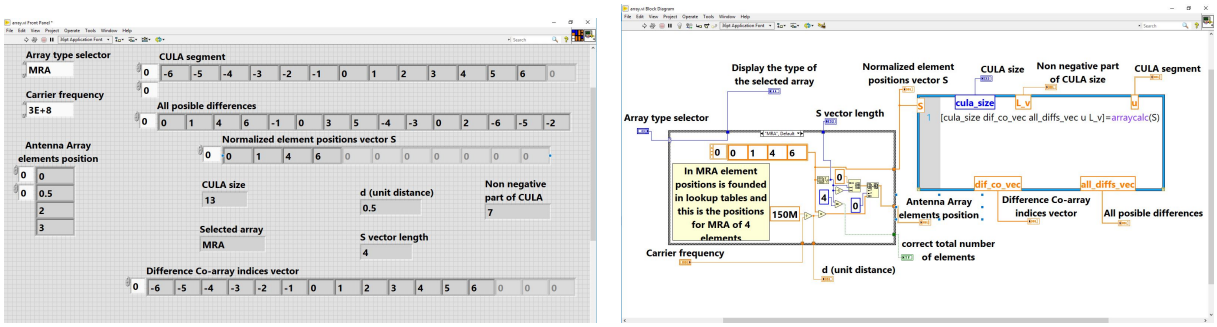

(A) SubVI front panel (B) SubVI block diagram

FIGURE 9. Design sparse antenna array structure SubVI

array structure" SubVI to the parameters identification loop, which is utilized to create the sparse array geometry. As illustrated in figure 9, this SubVI returns the DCA indices vector, the distance between array elements, the normalized element positions, the non-negative portion size of the CULA, the indices of the CULA segment in the DCOA, and its size in accordance with the chosen sparse array type, the design parameters of each type, and the number of physical elements in the array. Figure 9a represents this SubVI front-panel while figure 9b represents its LabVIEW block diagram graphical code that shows how MATLAB and graphical code are combined in the same LabVIEW program using a Math-Script Node. Secondly, we add a "virtual covariance matrix estimation" processing stage to the processing loop to perform the virtual array processing steps. In this stage, the DCA output is first estimated, and then the CULA segment output is extracted. Subsequently, spatial smoothing is utilized to estimate the virtual covariance matrix, which is then used by the MUSIC algorithm to estimate AOA. Reducing the mutual coupling effect and increasing the effective CULA part in the DCA for MRA over ULA improves estimation performance in terms of accuracy and resolution. This gives sparse-arrays-based AOA estimation a competitive edge over ULA-based AOA estimation.

TABLE 1. List of used components in DF experiment setup

Item	Version	Amount	Function
CPU	HP Core I7	1	Host for signal processing
USRP	NI USRP-2930	6	Four USRPs to form 4-channel receiver (Rx) one USRP is utilized as reference-signal transmitter one USRP is utilized as SOI transmitter
Clock distributor	OctoClock-G CDA-2990	1	LO synchronization in all Rx-USRPs Aligning ADC timestamp
Gigabit Ethernet Switch	TP-Link	1	Connect all USRPs to host PC
Software	LabVIEW 2019		Processing environment
Rf antennas	VERT400 Antenna 783074-01	5	Four antenna elements for the receiver one antenna element for SOI transmitter
Operating system	Windows 10		
power splitter	Mini-Circuits ZFRSC-4-842-S+	1	power splitting for the calibration process
Cables	SMA-M to SMA-M	17	For all connections illustrated in fig 7

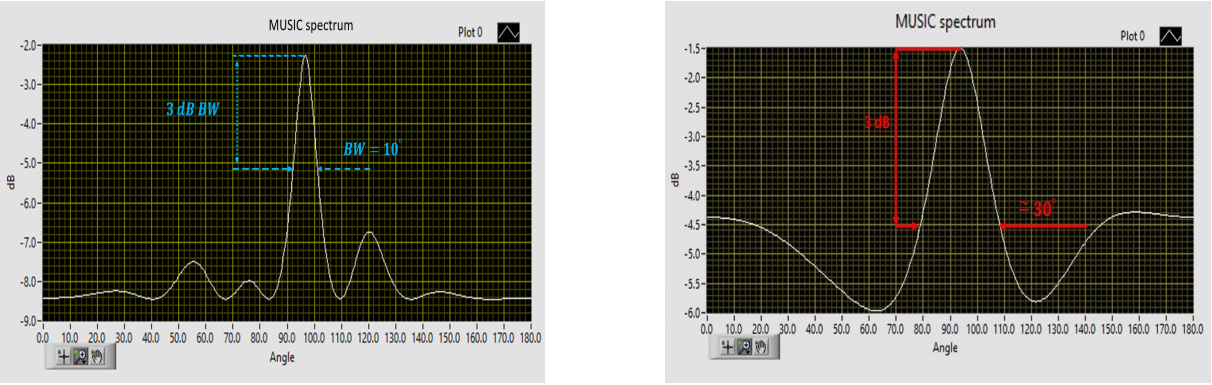

(A) Sparse array (B) ULA

FIGURE 10. Experimental validation results for DF based on sparse array Vs ULA

Previous outcomes ensured by the experimental results, in which the $3dB$ BW decreased from 30° in case of using ULA to 10° in case of MRA, as shown in figure 10.

5. **Conclusion.** In conclusion, this paper conducted a comprehensive analysis and practical implementation of sparse arrays versus ULAs for AOA estimation. The study commenced with a review of sparse array-based DF, exploring its idea of operation and its most well-known configuration types. Subsequently, a comparison between sparse arrays and ULAs was made, with the CRB serving as the metric for evaluating estimation performance. The theoretical study ensured the following findings: unlike NA and COA, which contain a closed-form equation, MRA lacks an equation for determining the sensor positions. However, it tries to maximize DCA while limiting the number of holes; when there is strong mutual coupling, COA is better, but it has a smaller DOF. In contrast, NA achieves larger DOF, which enhances estimated performance and resolution; nonetheless, NAs performance is significantly affected by the presence of strong mutual coupling. SNA seeks to overcome every drawback and maximize every benefit of the earlier types. Theoretical studies further confirmed that sparse arrays are less susceptible to mutual coupling compared to ULAs. They can achieve equivalent accuracy and resolution as ULAs while utilizing fewer antenna elements, resulting in reduced costs and complexity. Additionally, sparse arrays prove to be effective in dense environments, unlike ULAs. To reinforce the theoretical analysis, a simulation study was conducted. The simulation results corroborated the theoretical findings, further highlighting the superiority of sparse arrays over ULAs in terms of estimation performance. In this simulation, the DOF is 11, 27, 23, 15 and 23 for ULA, MRA, NA, COA and SNA, respectively. The simulation results demonstrated that SNA achieves the highest accuracy and resolution, with RMSE of 0.504°, followed by MRA, with RMSE of 0.55°, then NA and COA, respectively. On the other hand, ULAs exhibit the poorest accuracy and resolution, with an RMSE of 30.0477°. Consequently, SNA receives the highest rating, followed by MRA. The practical verification phase offered further validation for the effectiveness of sparse arrays using the NI-USRP SDR platform. This is evidenced by the decrease in the $3dB$ BW from 30° in ULA to 10° in MRA. The experimental results establish that sparse arrays consistently received the highest ratings when compared to ULAs. Our future study will focus on improving the estimation performance of sparse-array-based Direction finder in low SNR scenarios.

REFERENCES

[1] A. N. Abdullah and L. A. Abdul-Rahaim, "Comparative study of super-performance doa algorithms based for rf source direction finding and tracking," *Technology Reports of Kansai University*, vol. 63, no. 2, 2021.

[2] B. Boustani, A. Baghdad, A. Sahel, A. Ballouk, and A. Badr, "Performance analysis of direction of arrival estimation under hard condition," in *2018 4th International Conference on Optimization and Applications (ICOA)*, 2018, pp. 1–5.

[3] L. C. Godara, *Smart antennas*. CRC press, 2004.

[4] Y. Liao and A. Abouzaid, "Resolution improvement for music and root music algorithms." *J. Inf. Hiding Multim. Signal Process.*, vol. 6, no. 2, pp. 189–197, 2015.

[5] F. B. Gross, *Smart antennas with MATLAB®*. McGraw-Hill Education, 2015.

[6] C. S. Ateşavcı, Y. Bahadırlar, and S. Aldırmaz-Çolak, "Doa estimation in the presence of mutual coupling using root-music algorithm," in *2021 8th International Conference on Electrical and Electronics Engineering (ICEEE)*. IEEE, 2021, pp. 292–298.

[7] Y. Fang, S. Zhu, H. Wang, and C. Zeng, "Doa estimation via ula with mutual coupling in the presence of non-uniform noise," *Digital Signal Processing*, vol. 97, p. 102612, 2020.

[8] W. Hu and Q. Wang, "Doa estimation for uca in the presence of mutual coupling via error model equivalence," *IEEE Wireless Communications Letters*, vol. 9, no. 1, pp. 121–124, 2019.

[9] M. Wang, *Statistical Performance Analysis of Sparse Linear Arrays*. Washington University in St. Louis, 2018.

[10] C.-L. Liu and P. Vaidyanathan, "Super nested arrays: Linear sparse arrays with reduced mutual couplingpart i: Fundamentals," *IEEE Transactions on Signal Processing*, vol. 64, no. 15, pp. 3997–4012, 2016.

[11] G. Chen, B. Tian, J. Gong, and C. Feng, "Improving performance of direction-of-arrival estimation using sparse array in passive radar," *Journal of Algorithms & Computational Technology*, vol. 14, p. 1748302620943370, 2020.

[12] P. Pal and P. P. Vaidyanathan, "Coprime sampling and the music algorithm," in *2011 Digital signal processing and signal processing education meeting (DSP/SPE)*. IEEE, 2011, pp. 289–294.

[13] A. Patwari, "Sparse linear antenna arrays: a review," *Antenna Systems*, vol. 10, 2021.

[14] A. Jafri, "Array signal processing based on traditional and sparse arrays," Ph.D. dissertation, University of Sheffield, 2019.

[15] E. Epcacan and T. Ciloglu, "Analysis and comparison of coarray based sparse arrays," 2022.

[16] C.-L. Liu and P. Vaidyanathan, "Remarks on the spatial smoothing step in coarray music," *IEEE Signal Processing Letters*, vol. 22, no. 9, pp. 1438–1442, 2015.

[17] C.-L. Liu, "Sparse array signal processing: New array geometries, parameter estimation, and theoretical analysis," Ph.D. dissertation, California Institute of Technology, 2018.

[18] J. Shi, G. Hu, X. Zhang, and H. Zhou, "Generalized nested array: Optimization for degrees of freedom and mutual coupling," *IEEE Communications Letters*, vol. 22, no. 6, pp. 1208–1211, 2018.

[19] C.-L. Liu and P. Vaidyanathan, "Cramér–rao bounds for coprime and other sparse arrays, which find more sources than sensors," *Digital Signal Processing*, vol. 61, pp. 43–61, 2017.

[20] B. Friedlander, "On the cramer-rao bound for sparse linear arrays," in *2020 54th Asilomar Conference on Signals, Systems, and Computers*, 2020, pp. 1255–1259.

[21] M. Wang, Z. Zhang, and A. Nehorai, "Further results on the cramér–rao bound for sparse linear arrays," *IEEE Transactions on Signal Processing*, vol. 67, no. 6, pp. 1493–1507, 2019.

[22] O. Elkasrawi, A. Abdelaziz, H. AbouBakr, and M. Aboelazm, "Crb-based comparative study of array signal processing direction finding methods supported with sdr platform implementation," in *Journal of Physics: Conference Series*, vol. 2616, no. 1. IOP Publishing, 2023, p. 012039.